Available online at www.sciencedirect.com
ScienceDirect
Ceramics International 37 (2011) 2383–2390
CERAMICS INTERNATIONAL
www.elsevier.com/locate/ceramint

Hydrothermal synthesis of $BaTiO_3$ from different Ti-precursors and microstructural and electrical properties of sintered samples with submicrometric grain size

H.A. Ávila *, L.A. Ramajo, M.M. Reboredo, M.S. Castro, R. Parra

Instituto de Investigaciones en Ciencia y Tecnología de Materiales (INTEMA), UNMdP – CONICET, J. B. Justo 4302, B7608FDQ Mar del Plata, Argentina

Received 15 February 2011; accepted 21 March 2011
Available online 30 March 2011

Abstract

Barium titanate submicrometric particles were synthesized at 180 °C in a closed PTFE-lined stainless steel reactor with continuous stirring. Precursors used for titanium were Degussa P25 TiO_2 or titanium isopropoxide (TIP). Barium hydroxide ($Ba(OH)_2$) was added in a Ba/Ti = 1.1 molar ratio and KOH was used as mineralizer. The obtained powders were characterized by XRD and Raman spectroscopy. Powders were uniaxially pressed into discs and sintered at 1250 °C. The resulting microstructures were characterized by XRD, SEM, and Raman spectroscopy. Electrical measurements were carried out in order to characterize the ferroelectric behavior. The Ti precursor determined the sample density and grain size distribution and, consequently, the electrical response.

Keywords: C. Electrical properties; $BaTiO_3$; Hydrothermal; Microstructure

1. Introduction

Barium titanate, a perovskite type oxide, is the most popular ferroelectric material used in capacitors, piezoelectric and positive temperature coefficient devices. It is known that its ferroelectric behavior is associated with the displacement of Ti from its body-centered position in the lattice that causes a change in crystal symmetry, and that polycrystalline $BaTiO_3$ ceramics possess high dielectric constants when grains are bigger than 1 μm. However, the trend towards miniaturization and nanostructured devices made it necessary to evaluate the electrical response of barium titanate based on submicrometric and nanometric grains. A great deal of research has been carried out in order to determine the ultimate grain size that preserves this property, which strongly depends on crystalline structure [1,2].

In large grain (10 μm) ceramics, ferroelectric domains form to relieve the stress associated with the cubic to tetragonal transformation [3,4]. In order to explain the influence of grain size on the ferroelectric response, it was proposed that the dielectric constant of submicron (0.5–1 μm) grain-sized devices decreases because of substantial untwinning of the grains [5]. On the other hand, Clark et al. minimized the dependence of tetragonality with particle size [3]. Based on Raman studies, the authors showed that particles as small as 20 nm were tetragonal rather than cubic, contradicting the idea of a ''critical'' particle o grain size for the occurrence of asymmetry of TiO_6 octahedra [3]. Nevertheless, several studies based on X-ray diffraction also showed that the crystalline structure tends to cubic symmetry with crystallite size reduction. Recent reports showed that with decreasing grain size, the crystal structure at room temperature becomes progressively less tetragonal and the heat of the tetragonal to cubic transition is gradually reduced [6].

Solvothermal synthesis is considered an ideal method for low-cost production of ceramic powders at low temperatures, which yields ultrafine single crystals without any need for grinding, unlike many high-temperature techniques [7]. The key factors governing the chemical reactions in solvothermal processes have been recently reviewed by Demazeau [8]. Concerning the hydrothermal synthesis of $BaTiO_3$, the effects of temperature, time, pH, precursors and Ba/Ti ratio have been intensively studied

* Corresponding author. Tel.: +54 223 4816600.
E-mail addresses: havila@fi.mdp.edu.ar (H.A. Ávila), rparra@fi.mdp.edu.ar (R. Parra).

0272-8842/$36.00
doi:10.1016/j.ceramint.2011.03.032

during the last years [9–20]. For instance, Clark et al. suggested that amorphous titanic acid (H_2TiO_3) is an excellent precursor even though extended heating at 180 °C is needed for reaction completion [3]. Using TiO_2 and $Ti(OH)_4$, Chen and Chen found that particle size and morphology are strongly influenced by the Ti precursor [21]. They also observed morphology changes from clusters to spheres or cubes with increasing temperature. Titanium chloride ($TiCl_4$) has also been employed [22,23] and Komarneni and Katsuki recently used TiO_2 in microwave-assisted hydrothermal synthesis with very good results [24]. Barium precursors such as $BaCl_2$ [22,25–29], $Ba(OCOCH_3)_2$ [29–31], $Ba(NO_3)_2$ [26,29,32], and $Ba(OH)_2$ [3,21,33–37] have been evaluated. Dutta et al. determined that the amount of tetragonal content varies with the type of counterion in the order $I^- > Br^- > Cl^- > CH_3COO^- > NO_3^- > OH^-$, which coincides with the solubility order of the barium salts at 100 °C. Though the exact mechanism is not clear, the authors suggested that the most soluble salts promote the dissolution of $BaTiO_3$ perturbing the dissolution–recrystallization process [26].

In this work, $BaTiO_3$ was synthesized by a hydrothermal method with barium hydroxide and two sources of Ti: titanium isopropoxide and titanium dioxide. The obtained powders were pressed into discs and sintered resulting in samples with retention of the submicrometric grain size as in the *as synthesized* powders. Microstructural and electrical properties of powders and sintered samples were characterized.

2. Materials and methods

An alcoholic dispersion of 8.3 mmol of TiO_2 (Degussa P25) was added to an aqueous solution of 9.1 mmol of $Ba(OH)_2{\cdot}8H_2O$ (Ba/Ti = 1.1) inside a PTFE-lined stainless-steel reactor. The pH was fixed at 14 by the addition of 100 ml of a 1 M KOH aqueous solution. The same procedure was also carried out using titanium isopropoxide (TIP) instead of TiO_2. Titanium isopropoxide (97%, Aldrich) was dissolved in absolute ethanol and stabilized with anhydrous acetic acid (Cicarelli, 99.5%); the Ba/Ti ratio was also equal to 1.1. The closed reactor was heated at 180 °C, with constant stirring, in a silicon oil bath. After 24 h, the heating was stopped and the reactor was left to naturally cool to room temperature inside the oil bath. The resulting dispersions were washed with acetic acid in order to remove barium excess, possibly in the form of hydroxide and carbonate [38]. After washing several times with water, powders were left overnight at 60 °C for drying. Samples obtained from TiO_2 and TIP Ti-precursors will be referred to as BT-TiO_2 and BT-TIP, respectively.

The powders were characterized by X-ray diffraction (XRD, PANalytical X'Pert) and scanning electron microscopy (FE-SEM; Zeiss Supra 35). Powder patterns were registered under Cu Kα radiation from 10 to 80° 2θ with a step of 0.02° 2θ and data acquisition time of 0.5 s. In order to gain better resolution in the 44–47° 2θ range scans with 0.01° 2θ step size and acquisition times of 5 s were carried out. Raman spectra were acquired at room temperature with a Renishaw inVia microscope by means of the 514 nm Ar-ion laser line (50 mW nominal power) with a diffraction grating of 2400 lines/mm.

Afterwards, powders were uniaxially pressed into disks of 5 mm in diameter and 1 mm thick, approximately, and sintered at 1250 °C in a Carbolite furnace (equipped with an Eurotherm 2404 controller) with heating and cooling rates of 5 °C/min. The microstructural characterization of sintered and polished samples was completed by scanning electron microscopy (SEM; Jeol JSM-6460LV). The apparent density was measured by the Archimedes method. The crystalline phases present were assessed by XRD and Raman spectroscopy. In order to evaluate the electrical properties, measurements of capacitance were carried out at different temperatures with an HP 4284A impedance analyzer in the 20 Hz to 1 MHz frequency range using a Novocontrol BDS1200 sample cell. Polarization versus electric field hysteresis loops were obtained in a silicone oil bath at room temperature by applying an electric field of sinusoidal waveform at a frequency of 50 Hz by means of a modified Sawyer–Tower bridge.

3. Results and discussion

3.1. Powder characterization

The white powders found in the reactor after the syntheses consist in $BaTiO_3$ and are free from secondary or unreacted phases as shown by the X-ray diffraction patterns in Fig. 1. Independently of the Ti-source used, no traces of $BaCO_3$, TiO_2 or BaTiO-based phases (such as $Ba_6Ti_{17}O_{40}$) were detected. Regarding the crystalline structure, the cubic symmetry seems to dominate the XRD patterns. This is in agreement with the observations of Dutta and Gregg who demonstrated that using $Ba(OH)_2$ instead of $BaCl_2$ as source of Ba reduces the tetragonality of the final product [39]. On the other hand, it is known that chlorine ions are very difficult to rinse off and persist on the particles surface inhibiting densification during sintering.

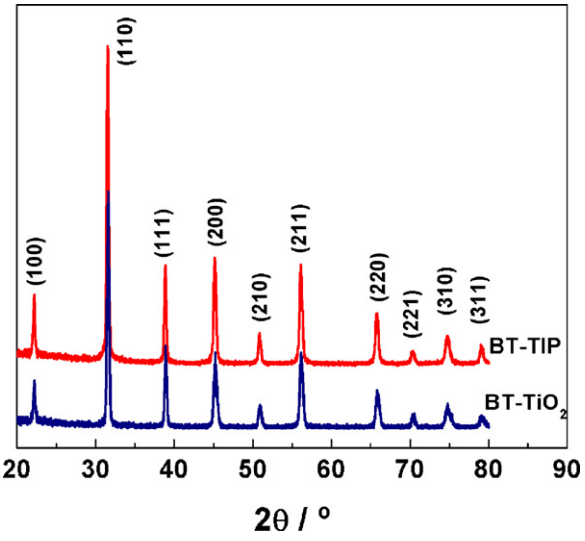

Fig. 1. XRD patterns of samples BT-TIP and BT-TiO_2 obtained by hydrothermal synthesis at 180 °C (assigned to $BaTiO_3$ according to the JCPDS 79-2263 file).

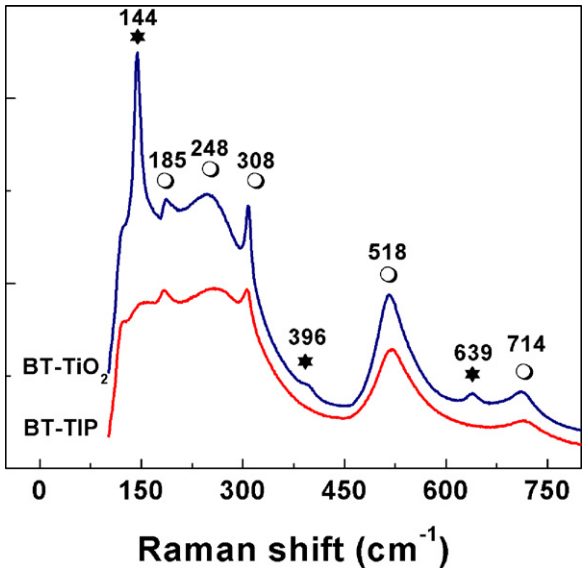

Fig. 2. Raman spectra of samples obtained by hydrothermal synthesis at 180 °C. Modes due to $BaTiO_3$ (○) and anatase (★) are indicated.

However, XRD is not as sensitive as to detect subtle variations in the structure of small crystalline regions. In fact, Raman spectroscopy led to different complementary conclusions. The spectra in Fig. 2 show the presence of $BaTiO_3$ in both samples and, interestingly, the peaks at 639, 396 and 144 cm^{-1} observed in the spectrum of sample BT-TiO_2 correspond to the anatase phase of TiO_2. This observation confirms that the reaction between $Ba(OH)_2$ and TiO_2 was not complete after 24 h and, the fact that anatase was not revealed by XRD, denotes that the unreacted TiO_2 amount must be very low and near the detection limit of the X-ray diffractometer. Traces of barium phases, other than $BaTiO_3$, were not detected neither by XRD or Raman spectroscopy. Furthermore, the Raman spectra in Fig. 2 clearly show the tetragonal distorsion of the $BaTiO_3$ structure. As it was pointed out by Robins et al., the narrow peaks at about 714 cm^{-1} and 308 cm^{-1} are specific to the tetragonal phase [40]. It can be concluded that in the BT-TiO_2 powder, both cubic and tetragonal phases of $BaTiO_3$ coexist along with traces of unreacted anatase.

The most accepted mechanisms for the hydrothermal or solvothermal synthesis of $BaTiO_3$ consist in the *in situ*

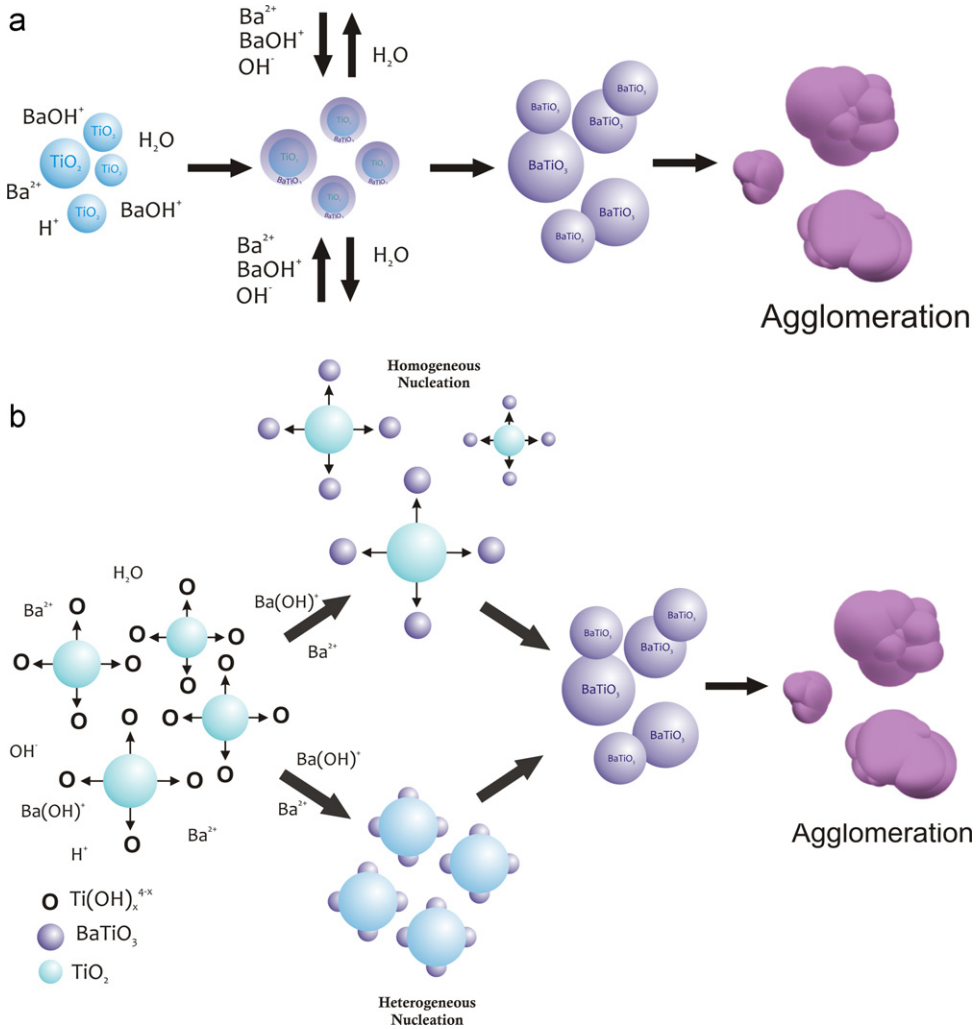

Fig. 3. Illustrative representation of (a) the *in situ* and (b) the dissolution precipitation reaction mechanisms that lead to $BaTiO_3$ under hydrothermal synthesis conditions (reproduced from Ref. [41]) including the agglomeration of particles or secondary nucleation stage.

transformation and dissolution–precipitation processes [41]. The former implies the reaction between TiO_2 and Ba ions or soluble complexes to form a $BaTiO_3$ layer through which barium must diffuse until the TiO_2 particle has completely reacted. According to the dissolution–precipitation mechanism, Ti–O bonds must be broken to form soluble Ti complexes that readily react with barium species to form $BaTiO_3$ [41]. Then, when P25 TiO_2 is used, there exists a homogeneous distribution of 30–40 nm crystalline particles (70% anatase, 30% rutile) well dispersed in the reaction medium since the beginning of the synthesis. Upon heating, OH^- ions promote the hydrolysis of Ti–O bonds on the particles surface followed by Ba^{+2} migration into the TiO_2 lattice and barium titanate crystallization on the surface of TiO_2 particles [39]. At a certain thickness, the layer may constitute a barrier to the diffusion of barium decreasing the $BaTiO_3$ crystallization rate and leaving unreacted anatase as detected by Raman spectroscopy and shown in Fig. 2. In addition crystalline titanium dioxide reacts slower than amorphous gels because of its lower solubility. Fig. 3a, which is based in the scheme proposed in the outstanding article by Eckert et al. [41], illustrates the transformation via the *in situ* mechanism.

On the other hand, when the KOH solution is added to titanium isopropoxide at room temperature, titanium hydroxide or oxyhydroxide gels precipitate from the solution. Upon heating, the gel is dispersed into primary particles such as $Ti(OH)_4$ or $Ti(OH)_6^{2-}$, among others, which condense with soluble Ba species in the medium. In this respect, Ba^{2+} and $BaOH^+$ have been suggested to be the most important species for barium in aqueous media at pH > 12 [42,43]. The higher reactivity of amorphous gels with respect to crystalline particles, leads to the rapid nucleation and growth of $BaTiO_3$ nuclei by means of dissolution–precipitation processes [3,41]. The scheme in Fig. 3b, as suggested by Eckert et al., illustrates the dissolution–precipitation mechanism [41].

Park and Park proposed that in the final stage the reaction is controlled by the solidification of aggregated particles [19]. However, Testino et al. had previously discarded the aggregative mechanism. Instead, they proposed a secondary nucleation process that explains the polycrystalline nature of the final particles, with the number of crystallites per particle increasing with the reaction time [43]. This gathering and rearranging of nuclei, or secondary nucleation, is now represented in Fig. 3a and b. A synthesis carried out at lower temperature evidenced the occurrence of this stage in $BaTiO_3$ formation. The image in Fig. 4, which corresponds to a SEM image of $BaTiO_3$ synthesized from titanium isopropoxide at 130 °C, shows how small particles agglomerate and solidificate into big polycrystalline particles. Because the formation of particles with narrow size distributions requires that the nuclei form simultaneously and without subsequent nucleation of smaller particles [44], there exists a compromise between monodispersity and reaction completion. Longer reaction times will lead to the formation of $BaTiO_3$ without the presence of anatase (when P25 is used) but will also lead to particle growth and polydispersity via aggregation of small particles.

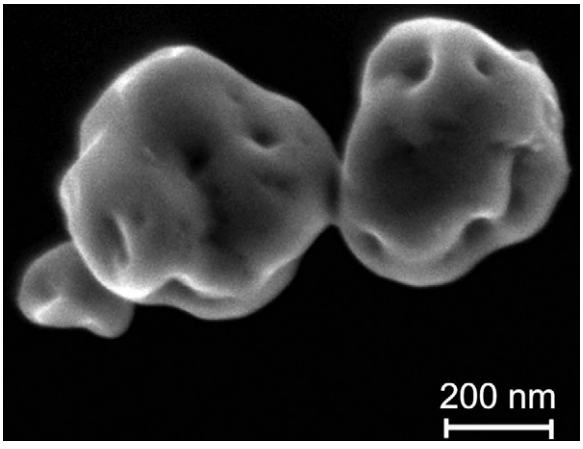

Fig. 4. SEM image of $BaTiO_3$ particles of a BT-TIP system synthesized at 130 °C showing how small particles aggregate into bigger particles.

3.2. Microstructural properties of sintered samples

The powder XRD patterns of samples sintered at 1250 °C shown in Fig. 5 demonstrate the sole presence of $BaTiO_3$. As observed in the XRD patterns of the *as synthesized* powders, these difractograms seem closer to the cubic than to the tetragonal phase. The inset in Fig. 5 shows that the diffraction peak associated with the (2 0 0) plane has not splitted into the (0 0 2) and (2 0 0) characteristic of tetragonal distorsion. It can also be observed that the (0 0 2) and (2 0 0) peaks may not have resolved due to the broadness of the peaks caused by the small crystallite size.

Nevertheless, as it was pointed out before, XRD is not the most appropriate technique to probe small crystalline regions. The existence of a significant degree of tetragonality was evidenced by micro-Raman spectroscopy. Two broad bands at

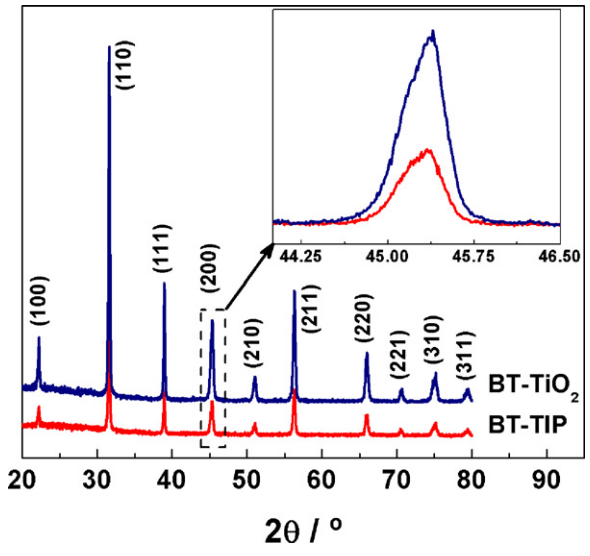

Fig. 5. XRD patterns of samples BT-TIP and BT-TiO_2 sintered at 1250 °C (assigned to $BaTiO_3$ according to the JCPDS 79-2263 file). Inset shows the profile of the diffraction corresponding to the (2 0 0) crystallographic plane of the cubic phase.

255 and 521 cm^{-1}, one weak band at 715 cm^{-1} and a sharp band at 309 cm^{-1} are clearly visible in the spectra of samples BT-TIP and BT-TiO_2 shown in Fig. 6. All the mentioned bands have been assigned to the tetragonal phase and seen to fade on heating above the Curie temperature of $BaTiO_3$ (~120 °C) as observed by several researchers [28,45,46]. Moreover, it was suggested that the peak near 185 cm^{-1} is observed for single-domain single-crystals of tetragonal $BaTiO_3$ [5]. The low intensity band at 650 cm^{-1} has been suggested to occur in small particle size samples or with a high density of grain boundaries such as in nanostructured polycrystalline films [45]. Other features in the spectra, relevant to phase identification, include a low intensity peak at 882 cm^{-1}, which has been rarely reported and has been assigned to a second order band of the mode at 440 cm^{-1} observed in $SrTiO_3$ [47,48]. The condition under which this mode appears is not clear.

A shoulder superimposed to the 521 cm^{-1} band at 490 cm^{-1}, usually assigned to rhombohedral and orthorhombic phases, can also be observed in Fig. 6 [45]. However, the positive intensity peak at 193–195 cm^{-1}, which would be indicative of the presence of orthorhombic phase, is not visible in the spectra of Fig. 6 [5]. In this case, as well as observed by Frey and Payne, Raman spectroscopy showed the occurrence of tetragonal distorsion in $BaTiO_3$ sintered samples apparently cubic according to XRD analyses [5].

The SEM images of sintered samples shown in Fig. 7 reveal the retention of the submicrometric grain size after thermal treatment and, therefore, the high density of grain boundaries as expected from Raman spectroscopy analysis. Both samples show porous microstructures with densities of 83% and 90% for

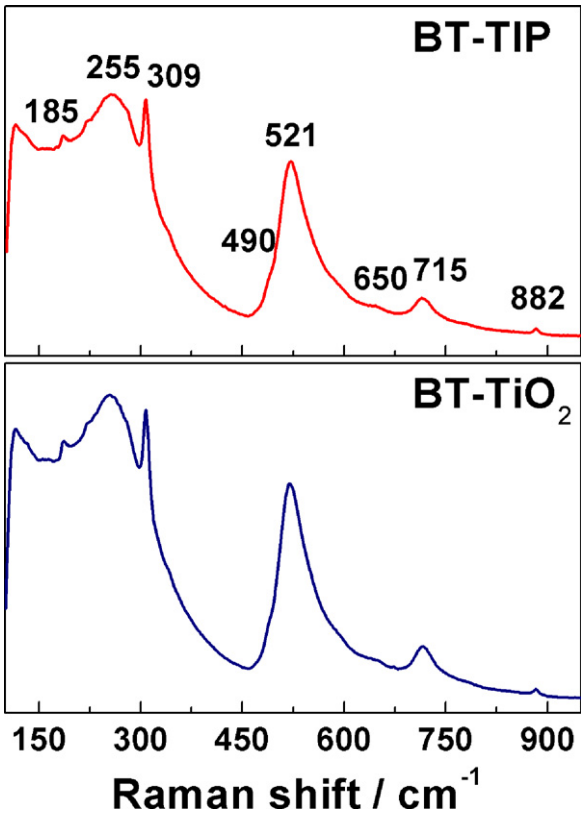

Fig. 6. Raman spectra of samples sintered at 1250 °C.

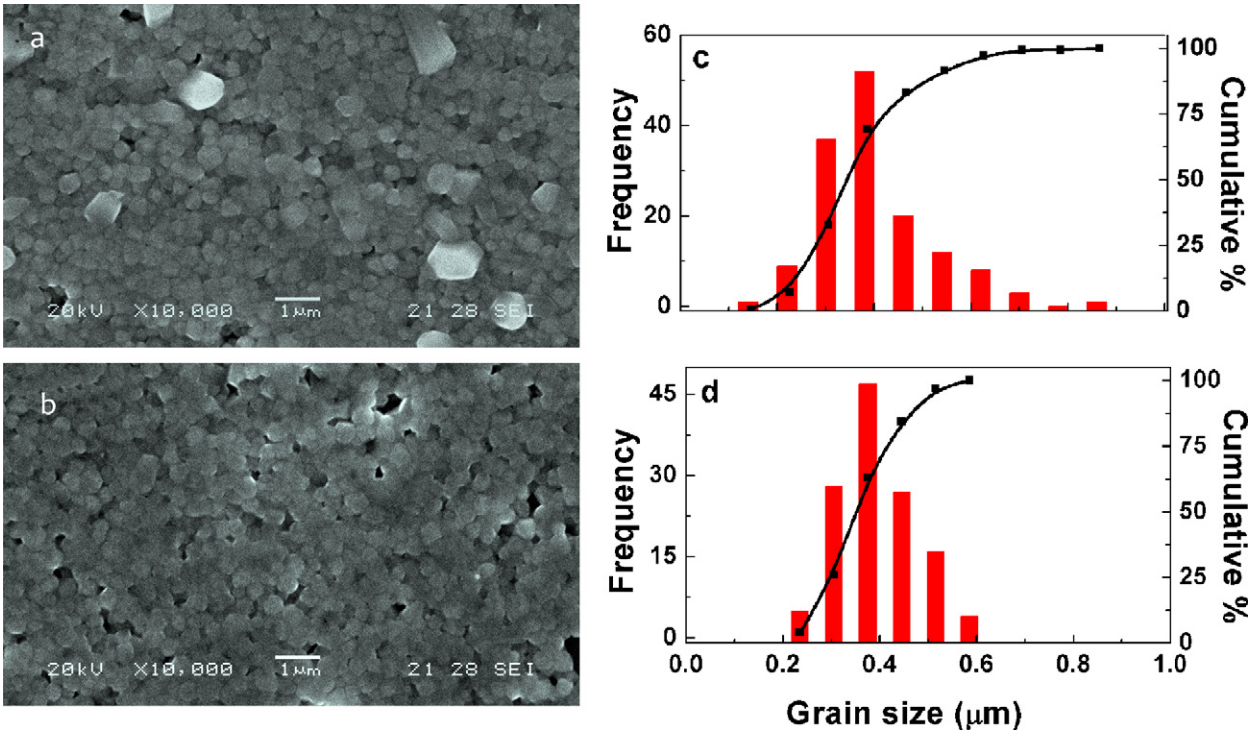

Fig. 7. SEM images and respective grain size distributions and cumulative curves for BT-TIP (a,c) and BT-TiO_2 (b,d) samples sintered at 1250 °C.

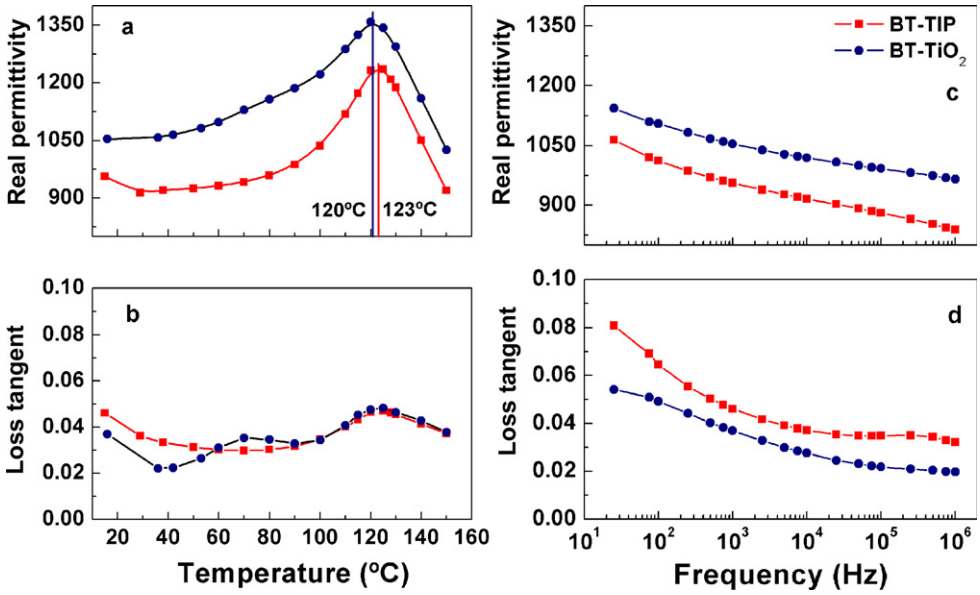

Fig. 8. Curves of the real part of permittivity and loss tangent versus temperature measured at 1 kHz (a; b) and of the same parameters as function of frequency at room temperature (c; d).

BT-TIP and BT-TiO_2, respectively. The relatively low sintering temperature led to low density values. However, at temperatures above 1250 °C the microstructure was severely damaged due to the formation of a liquid phase. From the histograms shown in the same figure, almost the same average particle size was determined for both samples; 0.40 μm for BT-TIP and 0.39 μm for BT-TiO_2. However, sample BT-TiO_2 showed a narrower size distribution with a lower dispersion than that of the BT-TIP sample.

3.3. Electrical properties of sintered samples

The BT-TIP sample showed a Curie–Weiss temperature T_c slightly higher than the BT-TiO_2 sample as seen in Fig. 8a, which shows the variation of the real permittivity with temperature. Interestingly, the permittivity curve for sample BT-TiO_2 is much broader than that for sample BT-TIP. Fig. 8b shows that both samples displayed low loss tangents with maximum losses around the T_c.

The real permittivity (Fig. 8c) showed higher values and lower losses (Fig. 8d) in the whole frequency range for sample BT-TiO_2. This sample showed a slightly higher permittivity value (ε_r = 1050 at 1 kHz) than the BT-TIP sample (ε_r = 950 at 1 kHz). Many studies have been carried out in order to determine the influence of the grain size on the dielectric properties of $BaTiO_3$ [2,49,50]. The general conclusion is that the dielectric constant decreases as the grain size is reduced from 10 μm to 1 μm [50]. However, if the grain size is further reduced (1 μm to 50 nm), the permittivity decreases significantly [2]. That is the reason for the low permittivity values measured for these samples. The influence of sample density on the permittivity is another parameter to be considered [51,52]. In fact, the introduction of nanopores in the microstructure of $BaTiO_3$ ceramics is an effective way to manipulate the dielectric constant especially in pyroelectric and piezoelectric applications where low dielectric constants are required [51]. Since the dielectric permittivity tends to decrease with increasing porosity, although the values measured for both samples are quite similar, the lower density of sample BT-TIP is responsible for the lower permittivity with respect to sample BT-TiO_2.

These results, specially the curves in Fig. 8a which show the symmetry change, confirm the existence of the ferroelectric tetragonal phase in both samples as predicted by Raman spectroscopy. This is in agreement with several reports that refuse the long accepted claim that the ferroelectric transformation is lost for grain sizes below 1 μm [3,5].

The studied samples exhibited ferroelectric behavior due to spontaneous polarization under an external strong electric field. Hysteresis loops of BT-TIP and BT-TiO_2 ceramics at room temperature under an *ac* electric field of E_p = 24 kV/cm at 50 Hz are shown in Fig. 9. The BT-TIP sample showed a remnant polarization (P_r) of 1.73 μC/cm^2, a higher value than

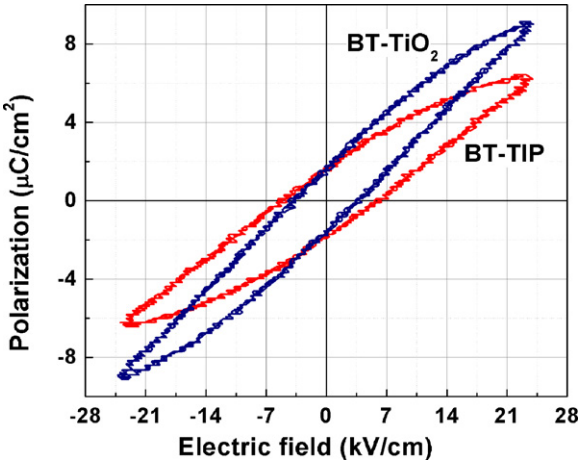

Fig. 9. Hysteresis loops of sintered samples at room temperature. Measuring conditions: *ac* field, electric field of 24 kV/cm and frequency of 50 Hz.

that measured for the BT-TiO_2 sample of 1.64 μC/cm^2. This is in agreement with the higher content of large grains (0.85 μm) and tetragonal structure of the BT-TIP sample, because a significant feature regarding the microstructures of ferroelectric ceramics is that larger ceramic grains typically contain larger and stable domains [53]. On the other hand, the higher saturation values (P_s) showed by the BT-TiO_2 sample (9.1 μC/cm^2) with respect to the 6.4 μC/cm^2 for the BT-TIP sample, can be attributed to the higher density or lower porosity content in this sample, which correlates with the permittivity curves in Fig. 8a and c.

4. Conclusions

Submicrometric $BaTiO_3$ particles were obtained by hydrothermal synthesis at 180 °C using titanium isopropoxide (BT-TIP) or titanium dioxide (BT-TiO_2), and barium hydroxide as precursors. Raman spectroscopy confirmed the crystallization in the tetragonal phase. Uniaxially pressed powders were sintered at 1250 °C retaining the submicrometric grain size. Samples showed ferroelectric behavior and tetragonal to cubic transition temperatures between 120 and 123 °C. The lower dielectric constant and the higher remnant polarization measured for sample BT-TIP are associated with the higher porosity and higher tetragonallity, respectively, with respect to the BT-TiO_2 sample. The source of titanium selected for the synthesis determined the microstructural properties of the sintered samples and, consequently, the electrical response.

Acknowledgements

This research was carried out with funds from CONICET and ANCyPT.

References

[1] S. Aoyagi, Y. Kuroiwa, A. Sawada, H. Kawaji, T. Atake, Size effect on crystal structure and chemical bonding nature in $BaTiO_3$ nanopowder, J. Therm. Anal. Calorim. 81 (2005) 627–630.
[2] V. Buscaglia, M.T. Buscaglia, M. Viviani, L. Mitoseriu, P. Nanni, V. Trefiletti, P. Piaggio, I. Gregora, T. Ostapchuk, J. Pokorný, J. Petzelt, Grain size and grain boundary-related effects on the properties of nanocrystalline barium titanate ceramics, J. Eur. Ceram. Soc. 26 (2006) 2889–2898.
[3] I.J. Clark, T. Takeuchi, N. Ohtoric, D.C. Sinclair, Hydrothermal synthesis and characterisation of $BaTiO_3$ fine powders: precursors, polymorphism and properties, J. Mater. Chem. 9 (1999) 83–91.
[4] I. Fujii, M. Ugorek, S. Trolier-McKinstry, Grain size effect on the dielectric nonlinearity of $BaTiO_3$ ceramics, J. Appl. Phys. 107 (2010) 104116.
[5] M.H. Frey, D.A. Payne, Grain-size effect on structure and phase transformations for barium titanate, Phys. Rev. B 54 (1996) 3158–3168.
[6] Z. Zhao, V. Buscaglia, M. Viviani, M.T. Buscaglia, L. Mitoseriu, A. Testino, M. Nygren, M. Johnsson, P. Nanni, Grain-size effects on the ferroelectric behavior of dense nanocrystalline $BaTiO_3$ ceramics, Phys. Rev. B 70 (2004) 024107.
[7] S. Komarneni, Q. Li, K.M. Stefansson, R. Roy, Microwave-hydrothermal processing for synthesis of electroceramic powders, J. Mater. Res. 8 (1993) 3176–3183.
[8] G. Demazeau, Solvothermal processes: definition, key factors governing the involved chemical reactions and new trends, Z. Naturforsch. 65b (2010) 999–1006;
G. Demazeau, A. Largeteau, S. Darracq, New trends in solvothermal crystal growth at the macro- and nanoscale, Z. Naturforsch. 65b (2010) 1007–1014.
[9] J. Moon, E. Suvaci, A. Morrone, S.A. Costantino, J.H. Adair, Formation mechanisms and morphological changes during the hydrothermal synthesis of $BaTiO_3$ particles from a chemically modified, amorphous titanium (hydrous) oxide precursor, J. Eur. Ceram. Soc. 23 (2003) 2153–2161.
[10] B.-K. Kim, D.-Y. Lim, R.E. Riman, J.-S. Nho, S.-B. Cho, A new glycothermal process for barium titanate nanoparticle synthesis, J. Am. Ceram. Soc. 86 (2003) 1793–1796.
[11] L. Qi, B.I. Lee, P. Badheka, D.-H. Yoon, W.D. Samuels, G.J. Exarhos, Short-range dissolution–precipitation crystallization of hydrothermal barium titanate, J. Eur. Ceram. Soc. 24 (2004) 3553–3557.
[12] M. Niederberger, G. Garnweitner, N. Pinna, M. Antonietti, Nonaqueous and halide-free route to crystalline $BaTiO_3$, $SrTiO_3$, and (Ba, Sr)TiO_3 nanoparticles via a mechanism involving C–C bond formation, J. Am. Chem. Soc. 126 (2004) 9120–9126.
[13] B. Hou, Z. Li, Y. Xu, D. Wu, Y. Sun, Solvothermal synthesis of single-crystalline $BaTiO_3$ nanocubes in a mixed solution, Chem. Lett. 34 (2005) 1040–1041.
[14] X. Zhu, J. Zhu, S. Zhou, Z. Liua, N. Ming, D. Hesse, $BaTiO_3$ nanocrystals: hydrothermal synthesis and structural characterization, J. Cryst. Growth 283 (2005) 553–562.
[15] P. Badheka, L. Qi, B.I. Lee, Phase transition in barium titanate nanocrystals by chemical treatment, J. Eur. Ceram. Soc. 26 (2006) 1393–1400.
[16] Y.V. Kolen'ko, K.A. Kovnir, I.S. Neira, T. Taniguchi, T. Ishigaki, T. Watanabe, N. Sakamoto, M. Yoshimura, A novel, controlled, and high-yield solvothermal drying route to nanosized barium titanate powders, J. Phys. Chem. C 111 (2007) 7306–7318.
[17] H.S. Lee, J.J. Lee, T.S. Chang, J.W. Kim, S.M. Koow, Hydrothermal synthesis for large barium titanate powders at a low temperature: effect of titania aging in an alkaline solution, J. Am. Ceram. Soc. 90 (2007) 2995–2997.
[18] Y. Hotta, C. Duran, K. Sato, T. Nagaoka, K. Watari, Densification and grain growth in $BaTiO_3$ ceramics fabricated from nanopowders synthesized by ball-milling assisted hydrothermal reaction, J. Eur. Ceram. Soc. 28 (2008) 599–604.
[19] J.H. Park, S.D. Park, Synthesis of barium titanate by hydrothermal method and its formation mechanism, J. Chem. Eng. Jpn. 41 (2008) 631–638.
[20] T. Kubo, M. Hogiri, H. Kagata, A. Nakahira, Synthesis of nano-sized $BaTiO_3$ powders by the rotary-hydrothermal process, J. Am. Ceram. Soc. 92 (2009) 172–176.
[21] H.-J. Chen, Y.-W. Chen, Hydrothermal synthesis of barium titanate, Ind. Eng. Chem. Res. 42 (2003) 473–483.
[22] A. Testino, M.T. Buscaglia, V. Buscaglia, M. Viviani, C. Bottino, P. Nanni, Kinetics and mechanism of aqueous chemical synthesis of $BaTiO_3$ particles, Chem. Mater. 16 (2004) 1536–1543.
[23] W. Sun, W. Liu, J. Li, Effects of chloride ions on hydrothermal synthesis of tetragonal $BaTiO_3$ by microwave heating and conventional heating, Powder Technol. 166 (2006) 55–59.
[24] S. Komarneni, H. Katsuki, Microwave-hydrothermal synthesis of barium titanate under stirring condition, Ceram. Int. 36 (2004) 1165–1169.
[25] S. Fuentes, R.A. Zárate, E. Chávez, P. Muñoz, M. Ayala, R. Espinoza-González, P. Leyton, Synthesis and characterization of $BaTiO_3$ nanoparticles in oxygen atmosphere, J. Alloys Compd. 505 (2010) 568–572.
[26] P.K. Dutta, R. Asiaie, S.A. Akbar, W.-D. Zhug, Hydrothermal synthesis and dielectric properties of tetragonal $BaTiO_3$, Chem. Mater. 6 (1994) 1542–1548.
[27] Y. Xie, S. Yin, T. Hashimoto, Y. Tokano, A. Sasaki, T. Sato, Mater. Res. Bull. 45 (2010) 1345.
[28] R. Asiaie, W. Zhu, S.A. Akbar, P.K. Dutta, Characterization of submicron particles of tetragonal $BaTiO_3$, Chem. Mater. 8 (1996) 226–234.
[29] X. Wang, B.I. Lee, M. Hu, E.A. Payzant, D.A. Blom, Nanocrystalline $BaTiO_3$ powder via a sol process ambient conditions, J. Eur. Ceram. Soc. 26 (2006) 2319–2326.
[30] S.-K. Lee, G.-J. Choi, U.-Y. Hwang, K.-K. Koo, T.-J. Park, Effect of molar ratio of KOH to Ti-isopropoxide on the formation of $BaTiO_3$ powders by hydrothermal method, Mater. Lett. 57 (2003) 2201–2207.

[31] H. Du, S. Wohlrab, M. Weiß, S. Kaskel, Preparation of $BaTiO_3$ nanocrystals using a two-phase solvothermal method, J. Mater. Chem. 17 (2007) 4605–4610.
[32] C. Chen, C. Li, Q. Su, Q. Peng, Large-scale synthesis of nanocrystals of barium titanate and other titanates through solution-phase processes, Mater. Res. Bull. 45 (2010) 1762–1767.
[33] N.C. Pramanik, S.I. Seok, B.Y. Ahn, Effects of reactant concentration and OH-[1] ions on the formation of nanocrystalline $BaTiO_3$ in solution, Mater. Res. Bull. 42 (2007) 497.
[34] P. Pinceloup, C. Courtois, J. Vicens, A. Leriche, B. Thierry, Evidence of a dissolution–precipitation mechanism in hydrothermal synthesis of barium titanate powders, J. Eur. Ceram. Soc. 19 (1999) 973–977.
[35] E. Ciftci, M.N. Rahaman, M. Shumsky, Hydrothermal precipitation and characterization of nanocrystalline $BaTiO_3$ particles, J. Mater. Sci. 36 (2001) 4875–4882.
[36] S. Yoon, S. Baik, M.G. Kim, N. Shin, Formation mechanisms of tetragonal barium titanate nanoparticles in alkoxide–hydroxide sol-precipitation synthesis, J. Am. Ceram. Soc. 89 (2006) 1816–1821.
[37] N. Sasirekha, B. Rajesh, Y.-W. Chen, Hydrothermal synthesis of barium titanate: effect of titania precursor and calcination temperature on phase transition, Ind. Eng. Chem. Res. 47 (2008) 1868–1875.
[38] K. Zhu, J. Qiu, K. Kajiyoshi, M. Takai, K. Yanagisawa, Effect of washing of barium titanate powders synthesized by hydrothermal method on their sinterability and piezoelectric properties, Ceram. Int. 35 (2009) 1947–1951.
[39] P.K. Dutta, J.R. Gregg, Hydrothermal synthesis of tetragonal barium titanate, Chem. Mater. 4 (1992) 843–846.
[40] L.H. Robins, D.L. Kaiser, L.D. Rotter, P.K. Schenck, G.T. Stauf, D. Rytz, Investigation of the structure of barium titanate thin films by Raman spectroscopy, J. Appl. Phys. 76 (1994) 7487–7498.
[41] J.O. Eckert Jr., C.C. Hung-Houston, B.L. Gersten, M.M. Lencka, R.E. Riman, Kinetics and mechanisms of hydrothermal synthesis of barium titanate, J. Am. Ceram. Soc. 79 (1996) 2929–2939.
[42] M.M. Lencka, R.E. Riman, Thermodynamic modeling of hydrothermal synthesis of ceramic powders, Chem. Mater. 5 (1993) 61–70.
[43] A. Testino, V. Buscaglia, M.T. Buscaglia, M. Viviani, P. Nanni, Kinetic modeling of aqueous and hydrothermal synthesis of barium titanate ($BaTiO_3$), Chem. Mater. 17 (2005) 5346–5356.
[44] B.L. Cushing, V.L. Kolesnichenko, C.J. O'Connor, Recent advances in the liquid-phase syntheses of inorganic nanoparticles, Chem. Rev. 104 (2004) 3893–3946.
[45] V. Buscaglia, M.T. Buscaglia, M. Viviani, T. Ostapchuk, I. Gregora, J. Petzelt, L. Mitoseriu, P. Nanni, A. Testino, R. Calderone, C. Harnagea, Z. Zhao, M. Nygren, Raman and AFM piezoresponse study of dense $BaTiO_3$ nanocrystalline ceramics, J. Eur. Ceram. Soc. 25 (2005) 3059–3062.
[46] T. Ostapchuk, J. Pokorný, A. Pashkin, J. Petzelt, V. Železný, D. Rafaja, I. Drbohlav, Soft-mode spectroscopy of $BaTiO_3$ thin films, J. Eur. Ceram. Soc. 25 (2005) 3063–3067.
[47] Q.-Y. He, X.-G. Tang, J.X. Zhang, M.-M. Wu, Raman study for $BaTiO_3$ system doped with various concentrations and treated at different temperatures, Nanostruct. Mater. 11 (1999) 287–293.
[48] P.S. Narayanan, K. Vedam, Raman spectrum of strontium titanate, Z. Phys. 163 (1961) 158–164.
[49] X.-H. Wang, R.-Z. Chen, Z.-L. Gui, L.-T. Li, The grain size effect on dielectric properties of $BaTiO_3$ based ceramics, Mater. Sci. Eng. B 99 (2003) 199–202.
[50] S. Guillemet-Fritsch, M. Boulos, B. Durand, V. Bley, T. Lebey, Electrical characteristics of $BaTiO_3$ ceramics from hydrothermal prepared powders, J. Eur. Ceram. Soc. 25 (2005) 2749–2753.
[51] R.Z. Hou, P. Ferreira, P.M. Vilarinho, Nanoporous $BaTiO_3$ crystallites, Chem. Mater. 21 (2009) 3536–3541.
[52] B. Ji, D. Chen, X. Jiao, Z. Zhao, Y. Jiao, Preparation and electrical properties of nanoporous $BaTiO_3$, Mater. Lett. 64 (2010) 1836–1838.
[53] S.-C. Lu, Y.-H. Chen, W.-H. Tuan, J. Shieh, C.-Y. Chen, Effect of microstructure on dielectric and fatigue strengths of $BaTiO_3$, J. Eur. Ceram. Soc. 30 (2010) 2569–2576.